applied optics

# Circuit level implementation of photonic crystal devices

MOHAMMAD HASAN REZAEI AND MOHAMMAD HASAN YAVARI*

*Faculty of Engineering, Shahed University, Tehran 3319118651, Iran*
**Corresponding author: mh.yavari@shahed.ac.ir*

*Received 17 April 2020; revised 13 September 2020; accepted 17 September 2020; posted 17 September 2020 (Doc. ID 395250); published 7 October 2020*

**Different types of photonic crystal components have been modeled by approximate RLC circuits. The proposed lumped circuits exploit the analogy of photonic crystal elements and RLC circuits. They are either coupled to each other or inserted like lumped circuits to imitate wave propagation within the photonic devices. Different examples such as side-coupled waveguide–cavity systems, side-coupled cavity–cavity systems, and improved structures are investigated for evaluating the theory. It is shown that the proposed circuits are exact enough to be substituted into the complicated calculations of numerical methods. In addition, the presented practical and straightforward procedure can be employed for flexible and efficient design. The results are verified using the finite-difference time-domain numerical simulations and coupled-mode theory for various devices.** 

https://doi.org/10.1364/AO.395250

## 1. INTRODUCTION

Integrated photonics is a promising platform for implementing large-scale mode transformations required for optical information processing [1]. According to the analogy between electronics and photonics, light control in optical circuits is similar to flow of electricity in electrical circuits. Optical devices show a faster speed, less energy consumption, and better stability than electrical circuits. The field of photonics is constantly advancing in developing optical integrated circuits, which use nano-cavities as switches for controlling the flow of light. Over the two last decades, photonic crystals (PhCs) have been extensively studied and several concepts such as the photonic bandgap, slow light, superprism effect, and negative refraction have emerged [2–5]. PhCs are used to realize optical devices, such as waveguides, splitters, resonators, optical filters, and optical switches [6–10]. Many studies have dealt with numerical and theoretical analysis of PhC devices. Different methods such as finite-difference time-domain (FDTD), time domain beam propagation [11], Dirichlet-to-Neumann [12], multiple multipole [13], theoretical method of coupled-mode theory (CMT) [14], etc., have been proposed. Among all of these methods, numerical methods, despite their generality and flexibility, need massive calculations and give us little insight into the physics of devices. In this regard circuit models are required, because of their efficiency in computation and their ability to provide physical insights. They bring the concepts and existing design methods of microwave area to optical PhC devices thereby improving our ability to design. Many circuit models have been proposed for active and passive optical devices: semiconductor lasers [15,16], optical amplifiers [17], photonic crystal devices [18], and Fano lasers [19].

The goal of this paper is to develop a more generalized circuit model (CM) based on previous works [20] for modeling various structures. Different models, such as the stub [21,22] and cascade models [23], are extensively covered. It is demonstrated that using these two models, different devices created based on PhC waveguides can be analyzed and optimized, but these models still have the problem of complexity when huge optical circuits are considered. Further, both the stub and cascade models complement each other and they cannot be used individually to describe more complicated circuits. In this paper, to our knowledge, for the first time we introduce an efficient and flexible modeling scheme for simulating (a) traditional PhC optical switches and (b) optical Fano switches. Optical Fano switches are a new type of switch which have Fano resonance instead of traditional Lorentzian resonance in their output spectrum. Indeed, Fano resonance, because of its asymmetric and high-quality factor shape, enables us to do switching operations while consuming less energy. Also, with these types of switches, we will be able to have optical femto-joule switches, which are required for future advanced optical devices [24]. Promising photonic systems for providing Fano resonances can be roughly classified into four classes: photonic crystal structures, arrays of coupled optical waveguide and resonators, plasmonic nano-structures, and metamaterials [25]. Recent advances on Fano resonances in plasmonic, photonic crystal, and metamaterial structures have been reviewed in [26–28]. In Fano devices, the interference of a discrete state with a continuum leads to asymmetric

peaks. This refers to the resonance scattering of quantum theory [29–31]. With regards to electric resonance, the electric-dynamic equations of the "sharp" and "broad" electric-resonant modes are established where Fano resonance emerges. Recently, several devices have been presented for providing this type of spectra. In this paper, we also used PhC structures and nano-cavities as building blocks of Fano devices, and different Fano structures are modeled based on circuit theory. The proposed structures can be used as high-speed all-optical switches as well as high-sensitivity sensors. Furthermore, the circuit model, which is a mapping image of the classical mechanics, can be employed toward Fano resonance concepts [32]. Inductance in passive electric circuits demonstrates an effect boosting with higher frequency, and the capacitance behaves in an opposite way.

Circuit models are typically used for simplifying simulations and deep physical analysis. Meanwhile, alternatively using simple models such as circuit models, numerical simulations (i.e., FDTD) can be done simply for various devices within a short time. Indeed, numerical models are mostly accurate but very complicated and heavy to calculate; thus, circuit models could be used to predict the behavior of the device, before simulations [33]. The method presented here has the advantage of straightforward modeling. Also, because of the flexibility of the model for lumped circuit like modeling, the model becomes a promising procedure for future huge optical circuit designs. Since the modeling capabilities of previous works to model huge and complicated structures are weak, to overcome the difficulties of section-based models, this paper illustrates a new element-based method to model different parts according to the elements of the structures with the problem addressed by employing an element-based procedure for modeling more complicated optical structures.

The paper is organized as follows. In Section 2, the procedure of the modeling is presented. Circuit implementations and modeling equations are described in Section 3. Section 4 deals with the discussion. Finally, Section 5 concludes the paper.

## 2. THEORY

To analyze optical devices, the discrete elements of photonic structures should be modeled individually after which the comprehensive model for photonic structures should be generalized. According to [34], an electric circuit analog of the photonic structure can be implemented. Obviously, capacitors play the role of charge storage devices while inductors act as flux storage devices. A standing wave is formed within the cavity which is responsible for the light confinement and because of the similarity of the concept to voltage storage in electronics, the equivalent element can be considered as a capacitor. On the other hand, the traveling wave formed in the waveguide is responsible for transmitting the light and because of the similarity of this concept to current storage in electronics, the equivalent element can be regarded as an inductor [Table 1 (A and B)]. Thus, there is an analogy between voltage and standing wave as well as between current and traveling wave.

We need to introduce capacitors as coupling elements [shown in Table 1 (C)] to describe the coupling effects between different optical elements with electronic analogs. Loss of the light to the air can be modeled as a resistor [Table 1 (D)] by supposing a dissipation of power in electronics since the resistor leads to electrical losses in forms of joule as with optical losses. In cavity-based structures, we have two types of optical losses due to cavities which should be considered in $Q$ factors. Apparently, the $Q$ factor consists of two different elements called vertical $Q_{\perp}$ and in-plane $Q_{\parallel}$ [35,36]. Vertical loss, i.e., $Q_{\perp}$, is independent of the elements around the cavity. This type of loss, which leads to a decline in the device performance, could be considered as an electrical resistance in the circuit model of the structure. Another part of the $Q$ factor ($Q_{\parallel}$) which is due to coupling to neighboring elements, can be modeled as a capacitor between two nodes in the circuit model, where each node is the equivalent of one optical element.

Because of the coupling effects between different optical elements, and due to optical loss of the waveguides and cavities, we need to model the optical elements by RLC circuits, i.e., $R$ is interpreted as loss of the cavities and $L(C)$ is conceived as traveling (standing) wave behavior of the elements.

Using the design procedure developed in this paper and Table 1, the circuit model can be implemented for optical structures. Generally, the presented concept can be used to design and model any other devices consisting of waveguides and cavities.

## 3. CIRCUIT MODEL IMPLEMENTATION

An appropriate line shape can be obtained by tuning the values of circuit model elements. In this method, we used parallel and serial compositions of $R$, $L$, and $C$ electrical elements for simulating each optical element. $R$ models the optical losses to the clad, $L$ is responsible for the traveling wave, and $C$ deals with local light confinement. Note that in cavities, inductance vanishes gradually due to the existence of standing wave while capacitance disappears gradually in waveguides due to existence of traveling wave. Nevertheless, by replacing optical elements with their equivalents, it is possible to model optical circuits with large-scale electrical circuits.

Side-coupled waveguide–cavity and cavity–cavity structures are key elements for realizing PhC devices [6,7,9,37,38]. For example, a cavity that is side-coupled to a PhC waveguide or another cavity could lead to Lorentzian resonances, or even sharp asymmetric resonances known as Fano resonances. Several optical structures are discussed here, and the circuit modeling is also described.

Initially, we investigate the behavior of parallel RLC circuits and compare the outputs with typical Lorentzian output spectra of optical devices. Then, several Fano structures as well as a new presented Fano structure will be modeled using electrical elements such as a resistor, inductor, and capacitor. Finally, CM results will be compared with FDTD results.

In the circuit model analysis, we used the input impedance of the circuit embedded in the single-input-single-output system. The transmittance is defined as $S_{21} = P_{\text{output}}/P_{\text{input}}$, where $P_{\text{input}}$ and $P_{\text{output}}$ are the input and output powers, respectively. By tuning the zeros and poles of the input impedance, we can implement appropriate asymmetric resonance toward simulating the preferred optical device. We employed the input impedance instead of oscillator-dynamic equations in the spectral domain to simulate the optical devices because of

**Table 1. Procedure of Circuit Modeling**

| | Element | Optical Equivalent | Electrical Equivalent | Symbol |
|---|---|---|---|---|
| A | Optical cavity | 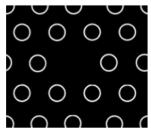 |  | $C$ |
| B | Waveguide | 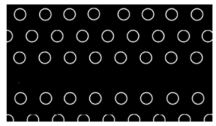 |  | $L$ |
| C | Coupling element | 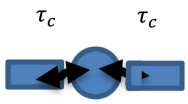  |  | $C$ |
| D | Loss to clad |   |  | $R$ |
| E | Perturbed waveguide | 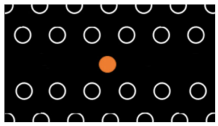 | 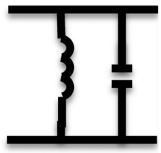 | $L_2, C_2$ |
| F | Low $Q$ Cavity | 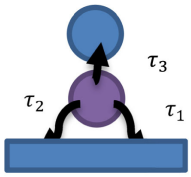  | 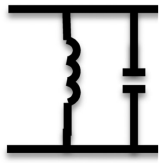 | $L_1, C_1$ |

simplicity and requirement of modeling, as well as tuning of the asymmetric and symmetric spectra, which is more feasible in the input impedance method [34].

The procedure of obtaining circuit model parameters includes the calculation of resonance frequency of photonic elements and deploying them to the circuit model and tuning the parameters toward fitting the results on FDTD/CMT plots while the resonance frequency is nearly the same.

### A. RLC Circuit for Making Lorentzian Spectrum

The first structure has been considered to be a typical PhC filter which has a Lorentzian spectrum at the output due to the cavity in the light path.

The bulk photonic crystal is made up of a triangular air hole photonic crystal slab with an air hole radius of 0.25a and thickness of 0.4a, where $a = 460$ nm [35,38]. The wavelength of light in the structure is the value typically used in optical communications. When the waveguide width is correctly defined (660 nm) to provide both low reflection and good optical confinement, the waveguide can be employed for single-mode operation. Note that the width is set smaller than usual to prevent excess waveguide mode from the output. The cavities are made through shifting two near holes in opposite directions with $S_1 = 85$ nm and second holes with $S_2 = 20$ nm (as shown in Fig. 1). The structure is simulated numerically with FDTD. The FDTD parameters are $\Delta x = 10$ fm and $\Delta t = 0.1$ fs. We used a simple RLC circuit for modeling the physical structure of Fig. 2(a). In this circuit [as shown in Fig. 2(b)], $R$ is used for modeling optical losses to the clad, $L$ is considered to model the traveling wave properties of the cavity, and $C$ is used for capturing the standing wave formation in the cavity. In Fig. 2(a), the up cavity is responsible for filtering the input light coming from the input waveguide.

The incident light from the input left waveguide transmits to the right output port at resonance frequencies of the up cavity with the Lorentzian spectrum emerging at the output waveguide [as shown in Fig. 2(c)]. There is one resonant photonic component, and thus only one RLC circuit is enough to simulate the behavior. $L$ and $C$ are key elements in simulating the structure as $R$ is applied to fit the result to physical limitations of the system. The LC system can be adjusted to make

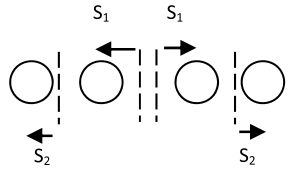


**Fig. 1.** Procedure of synthesizing the nano-cavity. $S_1$ and $S_2$ are shift vectors to shift PhC holes to make simple nano-cavity. Typical values of vectors are shown in Table 2.

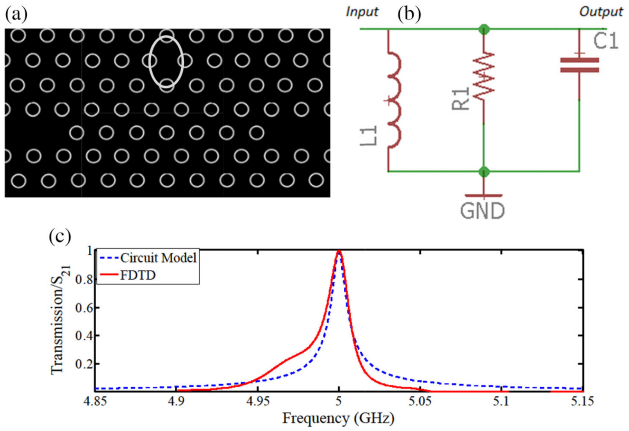


**Fig. 2.** (a) PhC Lorentzian optical switch structure containing one cavity and in/out waveguides. (b) Circuit model of the structure shown in part (a) (RLC circuit is responsible for Lorentzian filtering). (c) Comparison of the results of FDTD simulation and CM. The values of L, R, and C are 1.0132 pH, 20 TΩ and, 1 nF, respectively. The FDTD parameters are considered as $\Delta x = 10$ fm and $\Delta t = 0.1$ fs.

resonance at the preferred wavelength. In this structure, there is no mode interference (only one photonic resonant element exists) and no zero-pole adjustment is required to follow the FDTD results.

The equation that models the optical behavior of the PhC device shown in Fig. 2(a) is

$$Z = 1/\left(\frac{1}{R1} + \frac{1}{j\omega L1} + j\omega C1\right). \quad (1)$$

The results show that there is a good agreement between the circuit model results and numerical FDTD simulations [as shown in Fig. 2(c)]. The $R$, $L$, and $C$ values are extracted by considering the resonant frequency and bandwidth of the RLC circuit which are $1/\sqrt{LC}$ and $R/L$, respectively. The CM implemented here can be used to analyze complicated optical devices consisting of the side-coupled cavity–waveguide and cavity–cavity structures.

### B. Circuit Level Implementation of Fano Structure (Type I)

Two conventional PhC-based Fano structures have been introduced in [38,39]. The first structure is a two-cavity system blocking the waveguide for guiding light to the output port through two light paths via cavities [Fig. 3(a)]. In the PhC-based Fano resonator, a simple nano-cavity could represent the discrete state while the waveguide stands for the continuum. When the spectrum of the states is combined at certain frequencies, the Fano resonance will occur. Both the waveguides and cavities can play the role of continuum states [38,39]. Regarding the quality factor (QF), two elements with a high QF contrast interact and consequently, Fano resonance can take place. In the structure shown in Fig. 3(a) [29], a PhC nano-cavity-waveguide-based structure is used for making better light confinement toward better non-linear effects, and then smaller and lower energy consumption. The bulk photonic crystal structure is the same as the Lorentzian switch described in Section 3.A. The cavities

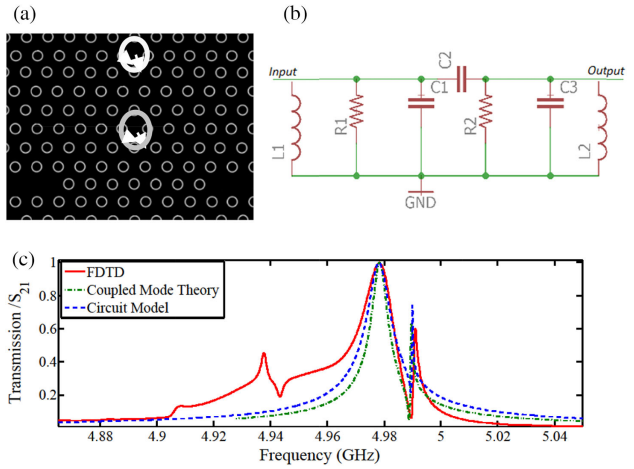


**Fig. 3.** (a) Optical PhC Fano switching structure Type I consisting of two cavities by applying the second cavity to achieve a Fano shape and in/out waveguides. (b) Circuit model of the structure; each RLC circuit is employed to model one cavity. The topological-induced difference of cavities is considered in R, L, and C values of each cavity model. (c) Comparing the results of FDTD, CMT, and CM. The FDTD parameters are considered as $\Delta x = 10$ fm and $\Delta t = 0.1$ fs. The values of $L_1$, $R_1$, and $C_1$ are 40.3443 pH, 150 Ω, and 1 nF, respectively. The values of $L_2$, $R_2$, and $C_3$ are 0.1268 pH, 85 Ω, and 317.480 nF, respectively. Also, $C_2 = 110$ pF.

**Table 2. Shifts Required to Make Cavities**

| | S1 | S2 |
|---|---|---|
| Cavity 1 (Down) | 85 nm | 20 nm |
| Cavity 2 (Up) | 90 nm | 20 nm |

of the structure shown in Fig. 3(a) have been made according to Fig. 1. The parameters of the cavities are reported in Table 2. Also, the waveguide width is set to 760 nm to have both a good confinement and proper light coupling. By setting the waveguide width to 760 nm, some unwanted modes which are due to entrapment of the light in the input waveguide (because of the small width of the device and photonic crystal devices as well as the vertical width of the input waveguide, which is nearly $a\sqrt{3}$ as with typical cavities in photonic crystal structures) have appeared at the output. These excess modes are not preferred and as such the waveguide width in the earlier Lorentzian structure, shown in Fig. 2(a), is set to 660 nm without any problem in functionality. The discussed modes are shown in the spectrum of Fig. 3(c) on the left tail of the FDTD plot which are not mimicked by theoretical circuit and CMT models. The excess modes were not considered in the theoretical models as they are unwanted effects.

The procedure for modeling the structure considers (1) an RLC circuit for each cavity and (2) a coupling capacitor for modeling the coupling that exists between elements. The final CM is shown in Fig. 3(b). Indeed, in resonant modes of cavities, the output is in its highest value while in off resonance, the output will be minimum with this behavior being in a good agreement with the results of the CM.

In the structure presented in this section, input light enters the structure from the left input waveguide and has two light

paths to follow. One path is through the down cavity while the other path is indirectly through the up cavity via the down cavity and then entering the output waveguide. Subsequently, the light is passed from two resonant elements with the light from different paths combined at the output waveguide, whereby interference occurs. The structure is considered as a structure with two resonant elements, while their resonances are close to each other. The equivalent circuit will be two LC circuits which are bound with a coupling element and have constructive and destructive interferences. According to the presented model, we should set zeros and poles of the circuit to have them in proper distance. Then, by adding $R_1$ and $R_2$ to both circuits, the desired Fano resonance appears. The model is adjusted, and its result is shown in Fig. 3(c).

The model is also evaluated by the FDTD and CMT, as displayed in Fig. 3(c).

The modeling equation for the CM is

$$Z = R_A + R_B + \frac{1}{j\omega C_2}, \tag{2}$$

where $R_A = \frac{1}{1/R_1+1/j\omega L_1+j\omega C_1}$, $R_B = \frac{1}{1/R_2+1/j\omega L_2+j\omega C_3}$, and $C_2$ is a capacitor for making coupling between two resonant states of the circuit. Also, the CMT equations for this structure are according to [38]

$$\frac{da_1}{dt} = \left(j\omega_1 - \frac{1}{\tau_{t1}}\right) a_1 + j\mu_1 a_2 + j\kappa_{CC} S_i, \tag{3}$$

$$\frac{da_2}{dt} = \left(j\omega_2 - \frac{1}{\tau_{t2}}\right) a_2 + j\mu_1 a_1, \tag{4}$$

where the resonance frequencies of the continuum and discrete states of the cavities are equal to $\omega_1$ and $\omega_2$, respectively; $a_1$ and $a_2$ indicate the field amplitudes of the down and up cavities; $\mu_1$ is the coupling coefficient between the first cavity and the waveguide; $S_i$ denotes the amplitude of light that couples to the structure; and $\tau_{ti}$ is the electric field decay rate and is calculated as

$$\tau_{t1}^{-1} = \tau_{t2}^{-1} = \tau_{\text{int}}^{-1} + \tau_{\text{cpl}}^{-1} + \tau_{\text{abs}}^{-1}, \tag{5}$$

where $\tau_{\text{int}}$ is the intrinsic decay rate of the cavity, $\tau_{\text{cpl}}$ denotes the coupling decay rate, and $\tau_{\text{abs}}$ is the absorption decay rate which is proportional to bulk material absorption. Also, by considering $S_{1+}$ as incoming light, $S_{1-}$ as reflecting light, and $S_{2-}$ as transmitted light, while the incoming light from the output is considered zero, the relation between in and out waves will be

$$S_{1-} = S_{1+} - \mu_1^* a_1, \tag{6}$$

$$S_{2-} = -\mu_2^* a_1, \tag{7}$$

where $\mu_1 = \sqrt{2/\tau_{\text{cpl}}} e^{j\theta_1}$, $\mu_2 = \sqrt{2/\tau_{\text{cpl}}} e^{j\theta_2}$, and $\kappa_{CC} = 2/\tau_{CC}$. $\theta_1$ and $\theta_2$ are either 0 or $\pi$ depending on the symmetric or antisymmetric property of the cavity mode profile, and $\kappa_{CC}$ can be calculated from $Q = \omega\tau/2$, where $Q_{CC}$ is the quality factor due to each of two coupled cavities.

The fitted transmission spectra of the CMT method, FDTD, and the presented circuit model are shown in Fig. 3, while the quality factors are obtained from experimental results, i.e., $Q_{cc} = 1800$, $Q_{\text{cpl}} = 3000$, $Q_{\text{abs}} = 34700$, and $Q_{\text{int}} = 10500$ [38]. The FDTD results are due to the interference between two different optical modes; with a one-by-one mapping, we could model each optical frequency mode induced from each cavity with a parallel RLC, as depicted in Fig. 3. Comparison of the results from the CMT, CM, and FDTD methods demonstrates the strength of the model in simulating this Fano-resonance-based structure. Thus, the circuit model as well as CMT and FDTD predict the behavior of the system and can be used to design optical circuits.

### C. Circuit Level Implementation of Fano Structure (Type II)

The second approach for making a Fano resonance is a simple structure introduced in [40]. The structure consists of a partially transmitting element (PTE) in a PhC waveguide coupled to a cavity (Fig. 4).

In the presented structure, a single cavity and a waveguide with a PTE with proper radius are resonant elements in the structure. By employing one or several PTE(s) or changing the PTE radius in the waveguide and also near the cavity, we could have different Fano resonances in terms of asymmetric property. Note that, adding extra PTEs or equivalently changing the PTE radius or vanishing PTE(s) leads to creation of a conventional Lorentzian spectrum at the output. Indeed, by adding PTEs (or changing the PTE radius), the waveguide reaches low quality factor ($Q$). Because of such a low-quality-factor cavity located in the vicinity of a real existing cavity, a stronger coupling between the cavity and waveguide will be obtained.

The result of the manipulation of the waveguide will be two optical paths shown in Fig. 4. Indeed, in this structure, by tuning the hole radius in the waveguide, the light coupled to the up cavity is tuned and we can switch between the Lorentzian and Fano spectrum. The circuit model of the structure could be modeled using the model presented in [34]. Switching between Lorentzian and Fano spectra could take place by tuning the capacitance of the coupling capacitor, which describes the coupling between the cavity and the waveguide in the structure (Fig. 5). By increasing the radius of the PTE inside the waveguide, the coupling of light to the cavity is increased. As a result, the second light path will be intensified [40]. Note that a simple circuit presented for the structure is implemented by employing the mentioned concept which comes from the analogy between electronics and photonics.

In the presented model, the light intensity in different paths could be tuned by modifying different elements in the model until Fano resonance occurs, and the important point is that we

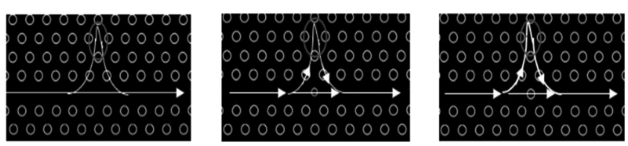

**Fig. 4.** Waveguide and a cavity that couples between them is tuned by changing the PTE radius in the waveguide and consequently, the Fano shape is changed. The first structure does not have any PTE and in the next structures, PTE is added and its size in increased respectively.

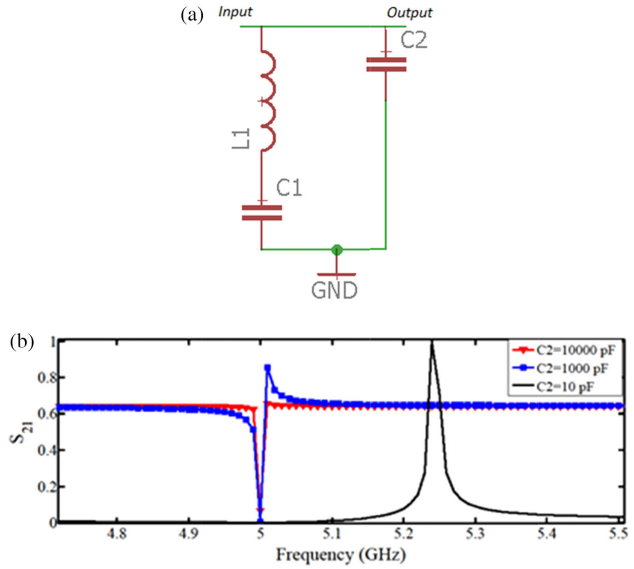


**Fig. 5.** (a) Circuit model of the presented structure in Fig. 4. This structure is implemented by a simple circuit. In the circuit, the capacitor and inductor are responsible for modeling the up cavity and capacitor ($C_2$) is applied for modeling the guiding element. (b) The change of PTE size in the waveguide is simply modeled by changing the $C_2$ capacitor in the model from 10 pF to 10000 pF; thus, the spectrum is reformed from Lorentzian to Fano shape and then came back to Lorentzian.

should refer it to coupling capacitor, i.e., $C_2$, phenomenologically. Because of the effect of adding PTE(s) (or equivalently changing its radius), which emerges as a transformation of waveguide to the low-$Q$ cavity, the series type of circuit model for the Fano structure shown in Fig. 3 could be applied for this structure, but the presented model is preferred because of the simplicity. In this model, the parallel RLC circuit which was the building block of the previous model is not used, and because of their differences in filtering mechanisms, just the series LC model is employed for modeling the structure.

### D. Circuit Model Implementation of the Proposed Fano Structure (First Stage Improvement)

We have proposed an improved Fano structure in [41,42]. Typically, the two-state system, which is crucial for making a Fano resonance, consists of two cavities with different $Q$ factors. Indeed, the up cavity, which has only coupling to the down cavity while its coupling to other elements is very weak, has a higher $Q$ factor with respect to the down cavity that is coupled to both of the waveguides and the up cavity. In the proposed structure, cavities are made by shifting two near holes and second ones around the cavity. The second shift is done for reducing the vertical losses of the cavity [38]. With regard to this mechanism, which is used for suppressing the loss, we suggest a new method which attempts to reduce the vertical losses as much as possible. Hence, the total $Q$ factor of the structure is increased, and the sharper Fano spectrum is produced.

The cavities of this structure are made according to Fig. 1 and Fig. 6(a). In other words, the new cavity discussed in this section, which is the discrete state in the structure, is made according to Fig. 6(a) to have a higher $Q$ factor than the continuum and the continuum state related cavity is made by Fig. 1. The parameters of the cavities are shown in Table 3.

In the presented method, the up cavity of the structure shown in Fig. 3(a) is more softened by symmetric shifting of more holes around the cavity, as discussed by Noda *et al.* [43]. The results of applying this method to the nano-cavity in the structure shows steeper Fano resonance due to reduction in vertical losses of the cavity. The down cavity remains unchanged. Applying this new method to nano-cavities leads to increasing $Q$ factor. The method of making the new cavity is shown in Fig. 6(a). For modeling an increase in $Q$ factor, a virtual cavity is considered in the position of up cavity (while its $Q$ factor is increased) [42]. The schematics of the presented method are shown in Fig. 6(b). The equivalent of the new cavity is modeled simply through repeating $R_B$ in the CM of Fig. 3(b). The CM is shown in Fig. 6(c). In this model, as discussed above, $R_2 = R_3$, $L_2 = L_3$, and $C_3 = C_4$. The equivalent circuit equation can be derived as below:

$$Z = R_A + 2 \times R_B + \frac{1}{j\omega C_2}, \tag{8}$$

where $R_A = \frac{1}{1/R_1 + 1/j\omega L_1 + j\omega C_1}$, $R_B = \frac{1}{1/R_2 + 1/j\omega L_2 + j\omega C_3}$, and $C_2$ is a capacitor for making coupling between two resonant states of the circuit.

The results of this circuit model in comparison to the CM of Type (II) structure (without any modifications) show better and steeper Fano shape at the output. The new structure with new cavity is also simulated with the FDTD method to confirm the model. The results of both FDTD and CM after the modifications are shown in Figs. 7(a) and 7(b), respectively. Comparing the two plots, it shows that the present results are in good agreement with FDTD results.

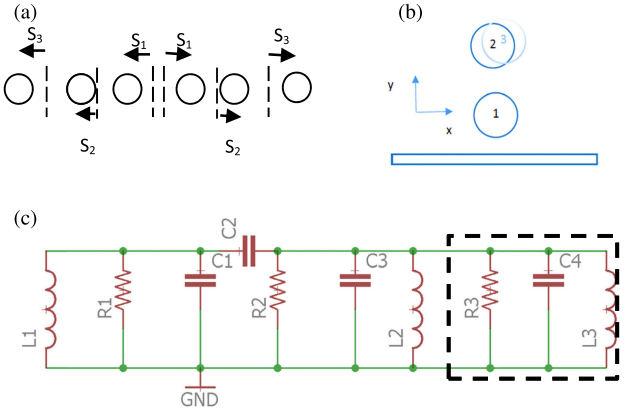


**Fig. 6.** (a) Procedure for making a new type of cavity. (b) Schematics of virtual cavity representation. (c) New structure equivalent circuit model; $R_2 = R_3$, $L_2 = L_3$, and $C_3 = C_4$.

**Table 3. Shifts Required for Making the Cavities**

| | S1 | S2 | S3 |
|---|---|---|---|
| Cavity 1 (up) | 92 nm | 11.5 nm | 92 nm |
| Cavity 2 (down) | 85 nm | 20 nm | 0 |

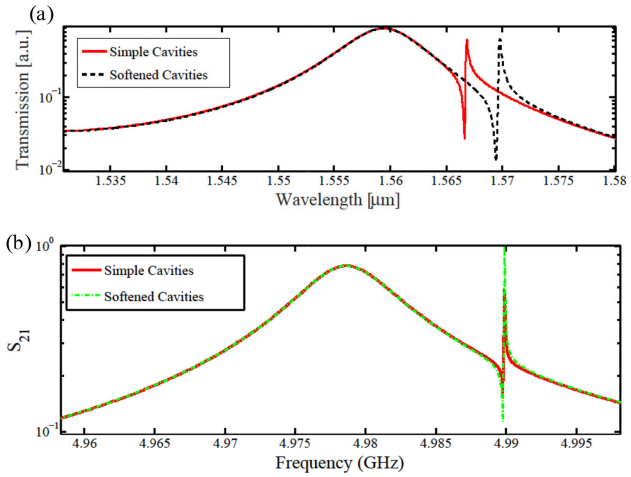


**Fig. 7.** (a) FDTD simulation results from the Fano structure. The FDTD parameters are considered as $\Delta x = 10$ fm and $\Delta t = 0.1$ fs. (b) Plots from output of the presented circuit model before and after applying the improving method.

### E. Circuit Model Implementation of the Proposed Fano Structure (Second Stage Improvement)

As shown in Fig. 8(a), for suppressing the losses of light induced from diffraction, the same two cavity systems are added into the region under the waveguide. Thus, the input light which is deviated into dual-cavity systems after collision with air holes in the waveguide is shaped and transmitted to the output. As discussed in [41,42], the new symmetrized structure consists of four cavities for manipulating the light and in/out waveguides for transmitting the light [Fig. 8(a)].

According to [41,42], employed cavities consist of two similar pairs of cavities while each pair is designed to make an asymmetric Fano shape. As such, two Fano resonances appear at the output. Note that waveguides are applied only for guiding

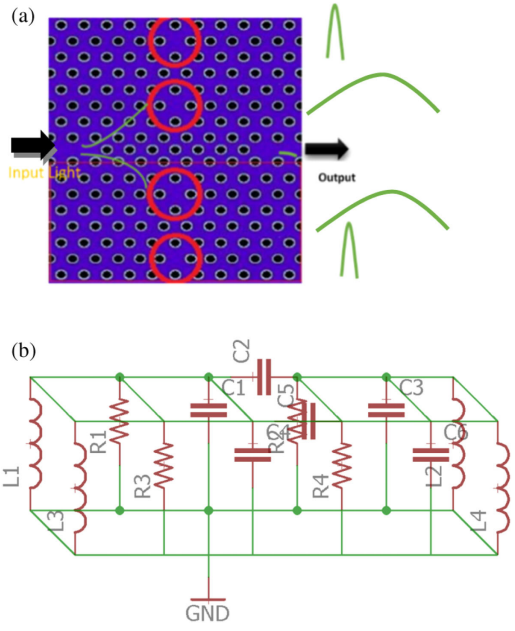


**Fig. 8.** (a) Symmetric structure, and (b) equivalent circuit model.

**Table 4. Shifts Required for Synthesis of Cavities**

| | S1 | S2 |
|---|---|---|
| Cavity 1 (up) | 85 nm | 20 nm |
| Cavity 2 (up) | 92 nm | 20 nm |
| Cavity 1 (down) | 85 nm | 20 nm |
| Cavity 2 (down) | 92 nm | 20 nm |

the light required to be switched to the structure. This symmetrization leads to greater increase of light transmission and reflection than previous structures when the switch is on and off, respectively. The cavities of the structure shown in Fig. 8(a) are made according to Fig. 1. The parameters of the cavities are shown in Table 4. The CM procedure for modeling the excess symmetric part is to double the circuit through paralleling it with the same circuit [shown in Fig. 8(b)]. When the same structure is added such that the input power is divided proportionally among components, it should be interpreted as paralleling the before circuit model with new component's circuit model. In this case, the new component is the same as the before structure. The equivalent circuit equation can be derived as Eq. (9):

$$Z = \left(R_A + R_B + \frac{1}{j\omega C_2}\right) \| \left(R_A + R_B + \frac{1}{j\omega C_2}\right), \quad (9)$$

while $R_A = \frac{1}{1/R_1 + 1/j\omega L_1 + j\omega C_1}$, $R_B = \frac{1}{1/R_2 + 1/j\omega L_2 + j\omega C_3}$, and $C_2$ is a capacitor for making coupling between two resonant states of the circuit.

Equations (8) and (9) describe how concepts are used to relate photonics and electronics.

The results of both FDTD and CM after two modifications discussed in Sections 3.D and 3.E are shown in Figs. 7(a) and 7(b), respectively.

## 4. DISCUSSION

Several different photonic elements, such as cavities, waveguides, cavity–waveguides, cavity–cavities, and other optical components have been discussed in previous sections. It can be said that the behavior of optical structures originates from the resonances and their interference; thus, and because of their simplicity and their ability to model these behaviors, electrical circuit models are desired. Comparison of results with the FDTD numerical method and also the CMT method shows a good agreement with experimental results.

Hence, the model makes it possible to analyze complicated optical circuits using electronic tools. In Sections 3.D and 3.E, the procedure of PhC optical structure modeling has been employed for simulating the effects of modifying the earlier devices. The comparison of the CM and FDTD simulation results, before and after the improvement, shows that the accuracy of the CM model is acceptable. According to [41,42], after improving the cavity responsible for the discrete state of the Fano system, the output Fano spectrum is sharpened. The modification is reflected to the CM by enhancing the part related to the modified cavity. The advantage of the model compared to other models is that, because of inserting the electrical analog of photonic components as lumped circuits, the modifications on

the structure can be applied to the circuit model just by modifying the related parts in the photonic structure. As another improvement action, the symmetrizing effect discussed in Section 3.E is applied to the CM, simply by paralleling the same circuit with the earlier CM. Indeed, the total system responsible for Fano is doubled, and therefore the equivalent modification will be doubling the circuit. The CM interpretation of the mentioned optical phenomena due to structural modifications of the photonic structure is presented as an example to show the ability of the CM to model future optical circuit challenges. Electronic interpretations of optical phenomena originate from the analogy between two areas and because of the element-based scheme employed in the presented model, other challenges around elements and phenomena could be addressed similarly. Every optical structure includes one or several elements, some of which are resonant elements and create the frequency behavior of the device. As shown in several sections, resonant elements can be substituted with electrical circuits where the relations between elements which are due to coupling phenomena should be addressed with the coupling element introduced above and then circuit modeling is straightforward. Fitting the results from the circuit model on the real device spectrum requires zero-pole analysis of $S_21$. Then, by adjusting the position of zero/poles to have a proper distance, the desired output is obtained. The presented scheme of modeling is practical and simple to use because of discrete designing and modeling, which are properties of lumped circuit modeling. Note that, as mentioned in Section 3.C, the parallel RLC model cannot always predict the behavior of the photonic device precisely. Indeed, in some cases where the transmission occurs in the off-resonant mode (in the opposite case where transmission occurs in the resonance mode), the series model is preferred. Thus, both circuit models are required for designs [Fig. 5(a)].

Comparison of the results with different numerical and theoretical methods such as FDTD and CMT shows a good agreement with the findings obtained from the circuit model presented here. The promised flexibility of the CM to consider future modifications on pre-designed optical circuits, which has not been addressed in earlier papers, will be crucial in optical interconnects. The other way to transfer designs from circuit models to optical structures is straightforward, where the device could be designed by the circuit model directly using Figs. 9(a) and 9(b).

These figures describe the frequency behavior of Lorentzian and Fano switches with respect to cavity sizes. They display the relationship between the cavity resonance frequency and related air hole shifts. Regarding $f = 1/\sqrt{LC}$, while $f$ is the resonance frequency, $L$ is the inductance, and $C$ is the capacitance of a resonant RLC electrical circuit and considering constant $L$, it is possible to calculate the $C$, and vice versa. Figure 9(a) has been drawn based on shifting two close air holes in the Lorentzian switch [Fig. 2(a)] by 80 to 90 nm, which is required for making nano-cavities. Figure 9(b) has been drawn by different shifts (up cavity) in the Type I Fano structure [Fig. 3(a)] on the horizontal axis and its resonance wavelength on the vertical axis. Note that Fig. 9(b) has been plotted by considering a constant shift of 85 nm of the down cavity. In both figures, wavelengths have been obtained from the FDTD method. As shown in

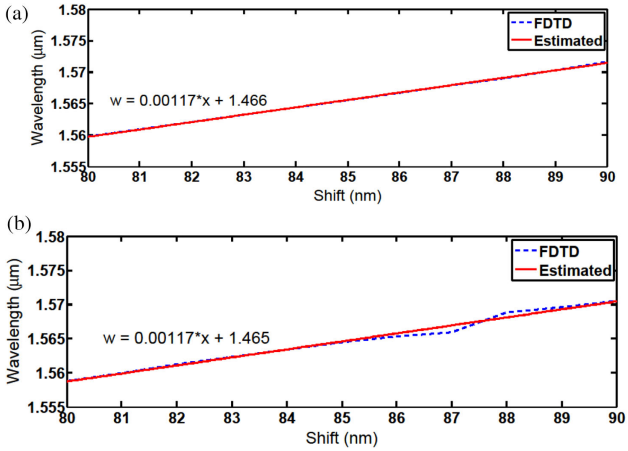


**Fig. 9.** (a) Required shift for predefined working frequency for the Lorentzian switch described in Fig. 2. (b) Wavelength versus required shift for designing the Fano switch described in Fig. 3.

both figures, shifts and resonance wavelengths are related by $w = 0.00117x + 1.47$. In this relation, the width of the origin of the equation, 1.47, shows the photoluminescence peak of the bulk material of the switch, which is the wavelength in zero shift ($x = 0$ in the above equation).

The slope of the line, 0.0017, shows the sensitivity of the structure to disordering, which is related to specifications. These figures have been plotted from FDTD simulations, and a linear equation has been estimated by fitting tools.

Depending on the Fano resonance shape, parallel or series RLC circuits are employed to describe the photonic structures. To describe Fano resonances with equal rising and falling tails, there is no difference between employing series or parallel RLC circuits. On the other hand, parallel RLC circuits have maximum impedance at resonance frequency, and they are appropriate to simulate the Fano resonances with a long tail at the rising part and a small tail at the falling part. The series RLC circuits have minimum impedance at resonance, and they are appropriate for another type of Fano resonance with a long tail at the falling part and a small tail at the rising part. Note that, when interference occurs between the continuum and discrete states, by approaching the tail of the continuum, the fully asymmetric Fano resonance occurs and because of limitations of falling effects at such frequencies, parallel RLC circuits cannot follow the Fano resonance with a long tail at the falling part. Also, similar behavior happens for a series RLC circuit. Consequently, as shown in Fig. 5, a series RLC circuit is employed for modeling the Type II Fano structure while a parallel RLC circuit is employed to simulate the Type I Fano structure (Fig. 3). It is noted that choosing the best circuit model based on the Fano resonance type is crucial in designing photonic circuits.

## 5. CONCLUSION

Considering future optical circuits involving cavities, waveguides, and a set of PTEs as well as material properties, it is possible to design the equivalent electronic circuit models of optical circuits which are the result of a deep understanding of analogy between electronic and photonic areas. Introducing

electronic models which are analogs of photonic elements beside phenomena (such as coupling, etc.), could open a new shared window in both electronics and photonics. In this paper, several elements and mechanisms were shared between electronics and photonics. We hope that the model presented herein will be useful in predicting the results of future optical designs before doing complicated numerical simulations. Further, this theoretical model could be useful to gain benefits of electronic circuit experiences in future optical computer designs (i.e., huge optical circuits). Another benefit of the presented method with respect to others such as CMT is that in this method, by adding a new element to the structure, it is not necessary to redesign and recalculate all computations. Also, we will work with electrical simulations instead of differential equations. Using this method, we can propose a design scheme for optical circuits.

**Disclosures.** The authors declare no conflicts of interest.

## REFERENCES


1. P. Mennea, W. Clements, D. Smith, J. Gates, B. Metcalf, R. Bannerman, R. Burgwal, J. Renema, W. Kolthammer, I. Walmsley, and P. Smith, "Modular linear optical circuits," Optica **5**, 1087–1090 (2018).
2. J. Joannopoulos, *Photonic Crystals* (Princeton University, 2008).
3. H. Kosaka, T. Kawashima, A. Tomita, M. Notomi, T. Tamamura, T. Sato, and S. Kawakami, "Super prism phenomena in photonic crystals," Phys. Rev. B **58**, R10096 (1998).
4. B. Gralak, S. Enoch, and G. Tayeb, "Anomalous refractive properties of photonic crystals," J. Opt. Soc. Am. A **17**, 1012–1020 (2000).
5. T. Baba, "Slow light in photonic crystals," Nat. Photonics **2**, 465–473 (2008).
6. M. Imada, S. Noda, A. Chutinan, M. Mochizuki, and T. Tanaka, "Channel drop filter using a single defect in a 2-D photonic crystal slab waveguide," J. Lightwave Technol. **20**, 873–878 (2002).
7. A. Yariv, Y. Xu, R. Lee, and A. Scherer, "Coupled-resonator optical waveguide: a proposal and analysis," Opt. Lett. **24**, 711–713 (1999).
8. X. Hu, Q. Gong, Y. Liu, B. Cheng, and D. Zhang, "Fabrication of two-dimensional organic photonic crystal filter," Appl. Phys. B **81**, 779–781 (2005).
9. M. Belotti, J. Galisteo-López, S. De Angelis, M. Galli, I. Maksymov, L. Andreani, D. Peyrade, and Y. Chen, "All-optical switching in 2D silicon photonic crystals with low loss waveguides and optical cavities," Opt. Express **16**, 11624–11636 (2008).
10. M. Bayindir, B. Temelkuran, and E. Ozbay, "Photonic-crystal-based beam splitters," Appl. Phys. Lett. **77**, 3902–3904 (2000).
11. M. Koshiba, Y. Tsuji, and M. Hikari, "Time-domain beam propagation method and its application to photonic crystal circuits," J. Lightwave Technol. **18**, 102–110 (2000).
12. Z. Hu and Y. Lu, "Efficient analysis of photonic crystal devices by Dirichlet-to-Neumann maps," Opt. Express **16**, 17383–17399 (2008).
13. J. Smajic, C. Hafner, and D. Erni, "Design and optimization of an achromatic photonic crystal bend," Opt. Express **11**, 1378–1384 (2003).
14. H. Haus and W. Huang, "Coupled-mode theory," Proc. IEEE **79**, 1505–1518 (1991).
15. P. V. Mena, " Circuit-level modeling and simulation of semiconductor lasers," Ph.D. dissertation (Illinois University, 1998).
16. M. Shekarpour, K. Saghafi, M. Jalali, and M. Yavari, "Circuit-level implementation of quantum-dot VCSEL," Opt. Quantum Electron. **48**, 355 (2016).
17. H. Ghafouri-Shiraz and B. Lo, *Distributed Feedback Laser Diodes* (Wiley, 1996).
18. A. Khavasi, M. Rezaei, M. Miri, and K. Mehrany, "Circuit model for efficient analysis and design of photonic crystal devices," J. Opt. **14**, 125502 (2012).
19. A. Zali, M. Moravvej-Farshi, and M. Yavari, "Small-signal equivalent circuit model of photonic crystal Fano laser," IEEE J. Sel. Top. Quantum Electron. **25**, 4900108 (2019).
20. S. Boscolo, M. Midrio, and C. Someda, "Coupling and decoupling of electromagnetic waves in parallel 2D photonic crystal waveguides," IEEE J. Quantum Electron. **38**, 47–53 (2002).
21. S. Boscolo, C. Conti, M. Midrio, and C. Someda, "Numerical analysis of propagation and impedance matching in 2D photonic crystal waveguides with finite length," J. Lightwave Technol. **20**, 304–310 (2002).
22. A. Khavasi, M. Miri, M. Rezaei, K. Mehrany, and B. Rashidian, "Transmission line model for extraction of transmission characteristics in photonic crystal waveguides with stubs: optical filter design," Opt. Lett. **37**, 1322–1324 (2012).
23. M. Miri, A. Khavasi, M. Miri, and K. Mehrany, "A transmission line resonator model for fast extraction of electromagnetic properties of cavities in two-dimensional photonic crystals," IEEE Photonics J. **2**, 677–685 (2010).
24. D. Miller, "Device requirements for optical interconnects to silicon chips," Proc. IEEE **97**, 1166–1185 (2009).
25. E. Kamenetskii, A. Sadreev, and A. Miroshnichenko, eds., *Fano Resonances in Optics and Microwaves: Physics and Applications* (Springer, 2018), Vol. **219**.
26. B. Luk'yanchuk, N. I. Zheludev, S. A. Maier, N. J. Halas, P. Nordlander, H. Giessen, and C. T. Chong, "The Fano resonance in plasmonic nanostructures and metamaterials," Nat. Mater. **9**, 707–715 (2010).
27. W. Zhou, D. Zhao, Y. Shuai, H. Yang, S. Chuwongin, A. Chadha, J. Seo, K. Wang, V. Liu, Z. Ma, and S. Fan, "Progress in 2D photonic crystal Fano resonance photonics," Prog. Quantum Electron. **38**, 1–74 (2014).
28. M. Rahmani, B. Luk'yanchuk, and M. Hong, "Fano resonance in novel plasmonic nanostructures," Laser Photonics Rev. **7**, 329–349 (2012).
29. U. Fano, "Effects of configuration interaction on intensities and phase shifts," Phys. Rev. **124**, 1866–1878 (1961).
30. A. Johnson, C. Marcus, M. Hanson, and A. Gossard, "Coulomb-modified Fano resonance in a one-lead quantum dot," Phys. Rev. Lett. **93**, 106803 (2004).
31. K. Kobayashi, H. Aikawa, A. Sano, S. Katsumoto, and Y. Iye, "Fano resonance in a quantum wire with a side-coupled quantum dot," Phys. Rev. B **70**, 035319 (2004).
32. S. Fan, W. Suh, and J. Joannopoulos, "Temporal coupled-mode theory for the Fano resonance in optical resonators," J. Opt. Soc. Am. A **20**, 569–572 (2003).
33. M. Yavari and V. Ahmadi, "Circuit-level implementation of semiconductor self-assembled quantum dot laser," IEEE J. Sel. Top. Quantum Electron. **15**, 774–779 (2009).
34. B. Lv, R. Li, J. Fu, Q. Wu, K. Zhang, W. Chen, Z. Wang, and R. Ma, "Analysis and modeling of Fano resonances using equivalent circuit elements," Sci. Rep. **6**, 31884 (2016).
35. K. Nozaki, T. Tanabe, A. Shinya, S. Matsuo, T. Sato, H. Taniyama, and M. Notomi, "Sub-femtojoule all-optical switching using a photonic-crystal nanocavity," Nat. Photonics **4**, 477–483 (2010).
36. T. Asano, B. Song, Y. Akahane, and S. Noda, "Ultrahigh-Q nanocavities in two-dimensional photonic crystal slabs," IEEE J. Sel. Top. Quantum Electron. **12**, 1123–1134 (2006).
37. S. Fan, "Sharp asymmetric line shapes in side-coupled waveguide-cavity systems," Appl. Phys. Lett. **80**, 908–910 (2002).
38. K. Nozaki, A. Shinya, S. Matsuo, T. Sato, E. Kuramochi, and M. Notomi, "Ultralow-energy and high-contrast all-optical switch involving Fano resonance based on coupled photonic crystal nanocavities," Opt. Express **21**, 11877–11888 (2013).
39. Y. Yu, W. Xue, H. Hu, L. Oxenlowe, K. Yvind, and J. Mork, "All-optical switching improvement using photonic-crystal Fano structures," IEEE Photonics J. **8**, 0600108 (2016).
40. Y. Yu, M. Heuck, H. Hu, W. Xue, C. Peucheret, Y. Chen, L. Oxenløwe, K. Yvind, and J. Mørk, "Fano resonance control in a photonic crystal structure and its application to ultrafast switching," Appl. Phys. Lett. **105**, 061117 (2014).

41. M. Rezaei and M. Yavari, "The proposal of new Fano structure for optical switching applications," in *Iranian Conference on Electrical Engineering (ICEE)* (2018).
42. M. Rezaei and M. Yavari, "Design and modelling of the photonic crystal Fano structure for all optical switching applications," Opt. Quantum Electron. **51**, 237–248 (2019).
43. Y. Akahane, T. Asano, B. Song, and S. Noda, "High-Q photonic nanocavity in a two-dimensional photonic crystal," Nature **425**, 944–947 (2003).